Chinese Chemical Letters 37 (2026) 111428

Contents lists available at ScienceDirect

Chinese Chemical Letters

journal homepage: www.elsevier.com/locate/cclet

Sustainable fungicide delivery *via* imazalil-functionalized nano-coordination polymer carriers: Enhanced stability, environmental safety, and pH-responsive properties

Gao-Sheng Zhu[a], Zhen-Hang Xu[a], Shao-Zhan Lan[a], Long Li[a], Yan-Ying Zheng[a], Lu Zhang[b], Qiao-Xia Shang[a], Bao-Yi Yu[a,*], Chong-Chen Wang[b,*]

[a] *Key Laboratory of Urban Agriculture in North China, Ministry of Agriculture and Rural Affairs, College of Bioscience and Resources Environment, Beijing University of Agriculture, Beijing 102206, China*
[b] *Institute of Advanced Materials/Beijing Key Laboratory of Functional Materials for Building Structure and Environment Remediation, Beijing University of Civil Engineering and Architecture, Beijing 100044, China*

ARTICLE INFO

Article history:
Received 2 February 2025
Revised 2 June 2025
Accepted 8 June 2025
Available online 8 June 2025

Keywords:
Nano-fungicide
Fungicide release
Antifungal activity
CP fungicide
Imazalil

ABSTRACT

The preparation of a novel nanoscale imazalil (IMZ)-based coordination polymer $[Zn(HBTC)(IMZ)_2]_n$ (**PDCP1**) ($H_3BTC = 1,3,5$-benzenetricarboxylic acid), and its antifungal application within a sustainable delivery system was reported. The intermolecular interactions presented in the structure, and their contributions to crystal packing were studied by Hirshfeld, Fingerprint plot and Mayer bond order. The obtained **PDCP1** had a relatively high loading rate of IMZ (68.5 %). **PDCP1** exhibited notable antifungal activities against *Colletotrichum gloeosporioides, Magnaporthe Oryzae*, and *Alternaria Nees* strains, with EC_{50} values of 0.72, 0.92, and 0.56 μg/mL, respectively. The key benefits of the application of **PDCP1** as a control release pesticide include high fungicide loading and offer nearly complete release, pH-responsive release, enhanced UV stability, exhibits favorable biosafety profiles. The remarkable inhibition of *C. gloeosporioides* growth by **PDCP1** underscores a promising strategy for agrochemical material development, high loading of active ingredients and readily delivery fosters more efficient pesticides utilization in agricultural processes.

© 2025 Published by Elsevier B.V. on behalf of Chinese Chemical Society and Institute of Materia Medica, Chinese Academy of Medical Sciences.

Imazalil (IMZ, 1-(2-(2,4-dichlorophenyl)-2-(2-propenyloxy) ethyl)-imidazole), as an imidazole based organic systemic fungicide [1,2], was extensively employed for the control of plant fungal diseases such as anthracnose [3], gray mold [4], and black spot [5], which commonly afflict fruits and vegetables [6]. The primary metabolic product of IMZ, imidazole ethanol (alpha-(2,4-dichlorophenyl)-imidazole-1-ethanol), is a compound known for its irritant properties [7–9], and prolonged exposure or high concentrations may cause skin and mucous membrane irritation [10]. Moreover, due to IMZ's poor thermal stability and high water solubility [11], conventional application methods often result in rapid environmental dispersal [12], leading to soil and aquatic contamination and reducing the fungicide's efficacy and utilization efficiency [13]. In particular, frequent and continuous application of IMZ may lead to environmental accumulation [14], potentially causing ecological toxicity [15] and promoting fungal resistance [16], thereby reducing the fungicide's long-term effectiveness [17]. Consequently, achieving long-term release of imidazole-based fungicides [18], especially in terms of maintaining high efficiency and minimizing toxicity, was of particular importance in agricultural chemistry [19].

Controlled-release has become a widely adopted strategy to address the limitations of conventional fungicide application by loading active ingredients within a carrier [20], further regulating the release of active compound to ensure the enhanced efficiency and prolonged effectiveness in protecting plants [21]. During the application, contact between the applicator, the environment, and the fungicide was minimized [22], while fungicide loss, which typically occurs through various dissipation pathways [23], was substantially reduced. To achieve the goal of long-term release [24], a fixed-loading system can effectively prevent the degradation of fungicide (*e.g.*, photolysis under ultraviolet light) [25]. The carriers used for fungicide loading included chitosan, hydrogel [26], cellulose, lignin, alginic acid, mesoporous silica, clay minerals, microcapsules and coordination polymers (CPs) [27–29]. Different from organic and inorganic carriers [30], CP-based carriers are advanta-

* Corresponding authors.
E-mail addresses: baoyi.yu@bua.edu.cn (B.-Y. Yu), wangchongchen@bucea.edu.cn (C.-C. Wang).

https://doi.org/10.1016/j.cclet.2025.111428
1001-8417/© 2025 Published by Elsevier B.V. on behalf of Chinese Chemical Society and Institute of Materia Medica, Chinese Academy of Medical Sciences.

geous due to their tunable structures and porosity [31], high specific surface areas [32,33], substantial loading capacity [34], and adjustable stability [35].

One strategy to achieve loading of a pesticide was application of the porous architecture of a CP material, which served as an encapsulation carrier [28]. Hou *et al.* [36] used the sol-gel method to synthesize a nanoparticle (Chl@UiO-66) with pH-responsive control release by loading chlorophyll (Chl) in UiO-66. This system enhances pesticide efficiency and reduces environmental impact. Yang *et al.* [37] modified ZIF-90 with β-CD-NH_2 and prepared a nanocomposite (IDC@ZIF-90-CD) with α-amylase and pH-responsive properties to control indoxacarb release. This material exhibits both insecticidal and fungicidal activities. Kobayashi *et al.* [38] successfully synthesized two CP-based materials derived from 1,4-dicarboxybenzene acid, Zn(II) and thiabendazole, which were used in control of *Escherichia coli*. Although these studies highlight the potential of CP-based carriers for responsive pesticide delivery and precise prevention and treatment, existing studies have neglected critical issues such as high cost, complicated synthesis process [39], poor stability [40], low loading rate [41], photostability [42], and potential ecological risks to aquatic organisms and mammals [43]. These areas remain essential for future investigation to ensure the broader applicability and safety of fungicide-based CP materials [44]. The development of controlled-release fungicide formulations has emerged as an effective strategy.

Herein, the fungicide-ligated coordination polymer **PDCP1** (Beijing University of Agriculture pesticide No. 1), formulated as $[Zn(HBTC)(IMZ)_2]_n$ (Fig. 1a), was synthesized through a reaction of IMZ, Zn(II), and H_3BTC in mixed solvents of DMA and water. Nano-sized **PDCP1** was synthesized using a stirring method, where a mixture of three stock solutions containing Zn(II), H_3BTC, and IMZ was vigorously stirred at room temperature for 2.0 h. And the obtained **PDCP1** contained a relatively high IMZ loading at 68.5 %, which surpassed the counterpart carriers (Table S1 in Supporting information). The dynamic light scattering (DLS) analysis showed that **PDCP1** particles exhibited an average size of 179 nm (Fig. 1b). The large-sized crystalline **PDCP1**, suitable for single crystal X-ray diffraction (SC-XRD), was obtained under static conditions at 80 °C over a period of 48.0 h. SC-XRD analysis revealed that **PDCP1** possessed a one-dimensional structure within the monoclinic crystal system (space group $P2_1/n$, No. 14). A summary of refinement parameters and crystal data (CCDC 2351489) (Fig. 1c), the selected bond lengths and angles, hydrogen bonding, X-H$\cdots\pi$, and $\pi\cdots\pi$ interactions, the supramolecular behavior of **PDCP1** were presented in Tables S2-S5 (Supporting information) and discussed in Supporting information.

The experimental powder X-ray diffraction (PXRD) patterns of **PDCP1** (synthesized under both static and stirred conditions) and the simulated one obtained from SCXRD were presented in Fig. 1d. The alignment of peaks positions among the patterns confirmed the phase purities of the CPs from all of the synthesis conditions. The charge state of **PDCP1** was evaluated to reveal the dispersion stability of the suspension by the zeta potential analysis. A higher absolute value of the zeta potential suggests greater suspension stability [45,46]. The synthesized **PDCP1** exhibited a zeta potential of 6.54 ± 0.23 mV in water (Fig. 1e), in comparison with a value of 1.66 ± 0.02 mV for the IMZ suspension. The thermal stability of **PDCP1** and IMZ was investigated using thermogravimetric analysis

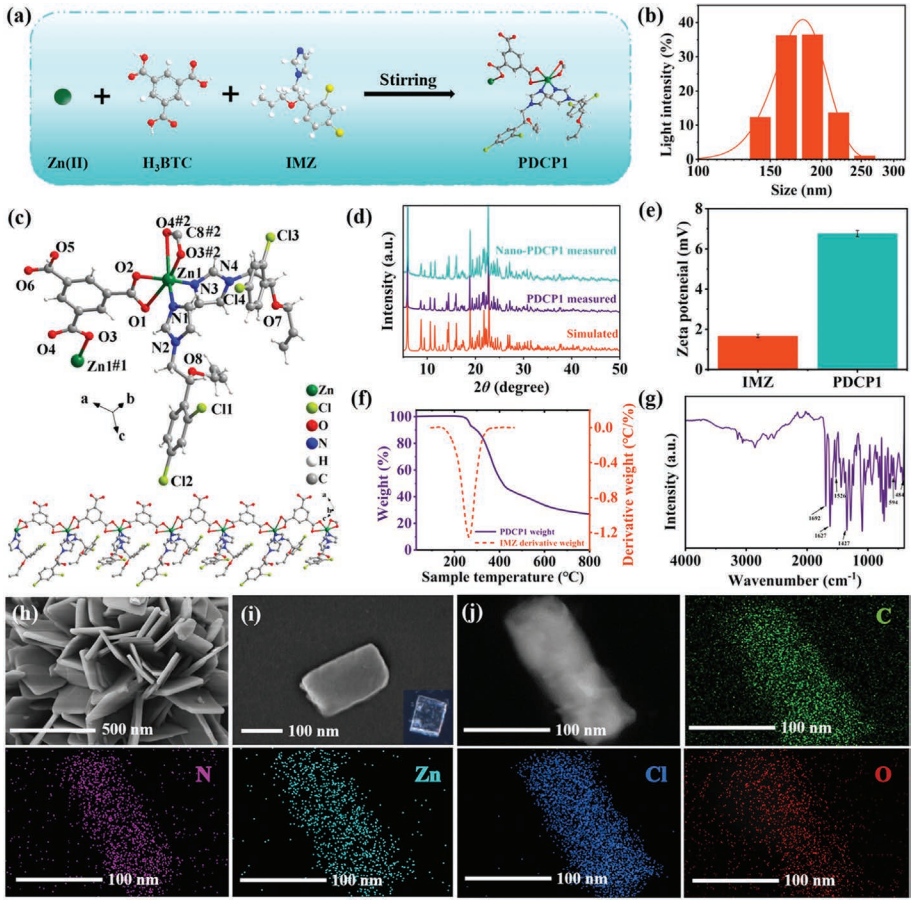


Fig. 1. (a) Schematic representation of the synthesis. (b) DLS analysis, and (c) coordination environment along with the 1D chain structure of **PDCP1**. Symmetry codes: (#1), $0.5+x$, $1.5-y$, $0.5+z$; (#2), $-0.5+x$, $1.5-y$, $-0.5+z$. (d) Simulated and experimental PXRD spectra, (e) zeta potential, (f) TGA spectrum for **PDCP1** and DTG spectrum for IMZ. (g) FT-IR spectrum, (h, i) SEM and (j) TEM images with EDS elemental mapping of C, N, Zn, Cl, and O of **PDCP1**.

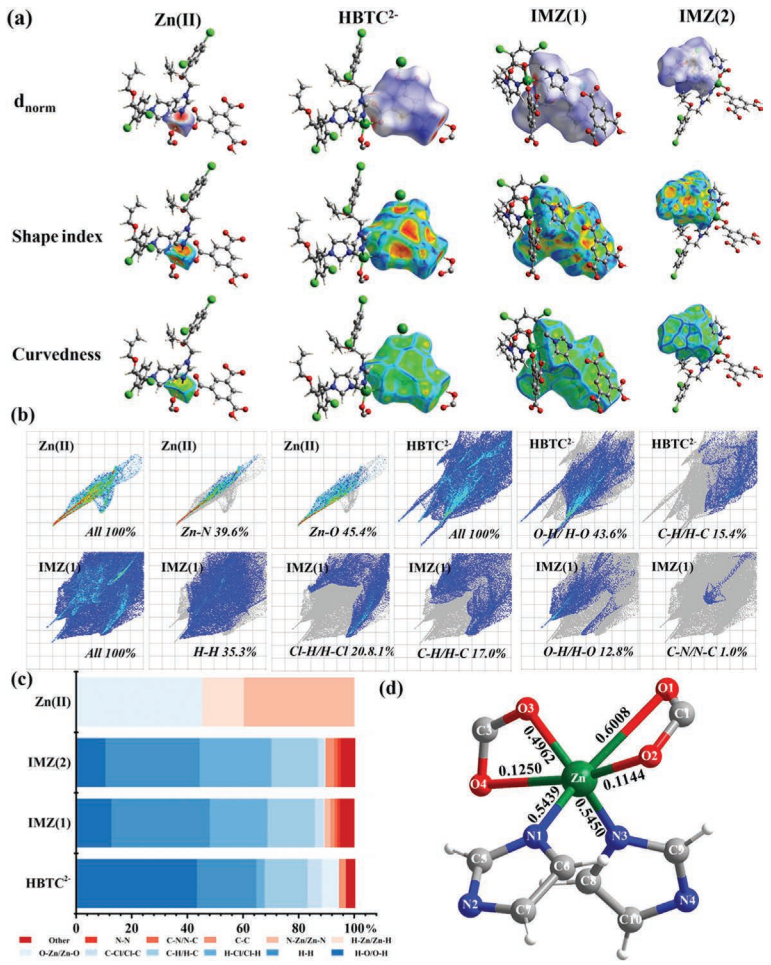


Fig. 2. (a) Hirshfeld surfaces mapped with d_{norm}, shape index, curvedness and (b) 2D fingerprints for Zn(II), IMZ(1), IMZ(2), and $HBTC^{2-}$. (c) Relative contributions of various interactions to the Hirschfeld surface of Zn(II), IMZ(1), IMZ(2), and $HBTC^{2-}$. (d) The Mayer bond order values of Zn-O and Zn-N in **PDCP1**.

(TGA) (Fig. 1f). The curve demonstrated that the sample mass remained relatively stable within the temperature range from room temperature to 260 °C. Above the temperature, a significant mass loss was observed, suggesting a thermal decomposition of the IMZ ligand started within the crystal structure. Additionally, TGA analysis of IMZ indicated that the derivative thermogravimetric (DTG) curve exhibited a peak at 260 °C [47], corroborating the suggestion. The Fourier transform infrared (FT-IR) spectrum of **PDCP1** was shown in Fig. 1g.

The morphology of nanosized **PDCP1** was investigated using scanning electron microscopy (SEM). As shown in Figs. 1h and i, individual plate exhibited a smooth surface and a relatively uniform lamellar shape. These plates clustered together to form a distinctive flower-shaped morphology [48], indicating a high degree of crystallinity and structural order within the material at a nanoscale. Further characterization was conducted using high-resolution transmission electron microscopy (TEM). The image of a single particle (Fig. 1j) revealed detailed physical features of the material. Complementary energy-dispersive X-ray spectroscopy (EDS) analysis was performed to assess the elemental compositions of the CP, confirming the presence and uniform distribution of the key elements: C, N, Zn, Cl, and O, suggesting a homogeneous composition throughout the nano-structure.

Hirschfeld analysis (HSA) was the electron density boundary surface between molecules in the crystal, and the intermolecular interactions inside and outside the surface could be clearly observed and analyzed (d_i and d_e represented the internal and external distances of the atoms from the interior to the HSA) [49–51]. Figs. 2a and b showed the HSA maps and 2D fingerprints of the individual components (Zn(II), $HBTC^{2-}$, IMZ(1), and IMZ(2)). And, the assembly of the four components was shown in Fig. S1 (Supporting information). The maps were generated using normalized contact distance (d_{norm}), shape index and curvedness, by which, the strong short-range interactions were shown in red, whereas the porous blue patches represent long-range intermolecular interactions. Blue areas therein indicated the proportion of the overall surface analysis accounted for the individual short-range interactions in 2D fingerprint [52]. The d_{norm} surface for Zn(II) exhibited intense red spots, which suggested strong interaction regions for Zn-O and Zn-N bonds, with 45.4 % and 39.6 % of the total Hirshfeld surface (Figs. 2b and c), respectively, and the rest 15.0 % was contributed from Zn···H interaction. Moreover, in addition to Zn-O, strong interactions in the d_{norm} map of $HBTC^{2-}$ presented of O–H···O hydrogen bond [53], which also exhibited a significant two sharp symmetric peaks in the fingerprint plots, accounting for 43.5 % of the total Hirshfeld surface. Shape index maps of IMZ(1) and IMZ(2) (Fig. 2a) possessed similar Hirschfeld forces, besides the Zn-N interactions, red and blue triangular regions in the shape index plot coincided with the $\pi\cdots\pi$ stacking interactions among the imidazole rings and the benzene ring from the two IMZ ligands, accounting at 3.5 % for IMZ(1) (C–C: 1.5 %, C–N/N–C: 1.0 %; N–N: 1.0 %), and 3.3 % for IMZ(2) (C–C: 3.0 %, C–N/N–C: 1.3 %; N–N: 1.2 %). In the curvedness graph, dark blue edges signify regions of high curvedness, while green edges indicated by flat areas, also

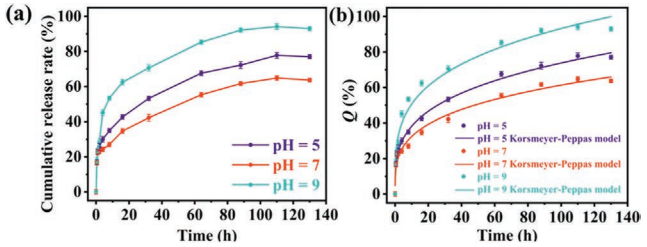


Fig. 3. (a) Cumulative release rate curve and (b) Korsmeyer-Peppas kinetic release model of the rates.

associated with $\pi\cdots\pi$ interactions [54]. Fig. 2c provided a summary of the relative contributions of various intermolecular interactions and the Mayer bond analysis (Fig. 2d, Figs. S1 and S2 in Supporting information) were discussed in Supporting information.

To investigate the release property of IMZ from **PDCP1**, an aqueous medium was investigated for consideration of real application. Fig. 3 showed cumulative released IMZ over time at different pHs (5, 7, and 9). The concentration of IMZ was determined using HPLC, based on the IMZ standard curve ($R^2 = 0.9999$) (Fig. S3a in Supporting information). As shown in Fig. 3a, IMZ was rapidly released from **PDCP1** within the first 8.0 h under all tested pHs, either the cumulative release rate under the conditions of pH 9 and pH 5 surpassed that of under the condition of pH 7. Under pH 9, the cumulative release rate reached 85.4 % at 64 h and stabilized at 94.3 % by 120.0 h; Under pH 5, 67.6 % of IMZ from **PDCP1** was released at 64 h, reaching 77.8 % at 120.0 h. Under a neutral environment, the release rate reached 55.3 % after 64 h and 64.8 % after 120.0 h. Furthermore, the cumulative release experiment in a lower concentration of **PDCP1** was performed and the result (Fig. S3 in Supporting information) showed that the IMZ in supernatant in concentration of 65.36 μg/mL after 60.0 h, and the cumulative release rate reached 98.1 % after 130.0 h (based on the percentage of IMZ in **PDCP1**, 68.5 %), indicating a good total delivery performance of the material. A comparison of the pH responsive pesticides release behavior of **PDCP1** and published carriers for imidazolyl-based fungicides (IMZ and PRO) are shown in Table S1.

The release mechanisms of organic ligands from CPs differ fundamentally from those observed in porous inorganic materials or polymeric systems [21]. In the mesoporous silica carriers [55], drug release typically occurs through pH-responsive bond cleavage at the pore surface, followed by passive diffusion through the silica matrix. Polymeric fungicide delivery systems, by contrast, predominantly rely on matrix-swelling [56] dynamics or hydrolytic/enzymatic degradation [57] of chemical bonds under specific physiological conditions. Regarding CP-based delivery platforms, the release of loaded pesticides reveals two distinct pathways [58]: (1) Structural dissociation of the coordination framework and (2) controlled diffusion through crystalline channels. Considering the stimuli of pH-responsive release behavior of IMZ from **PDCP1**, at a low pH, fungicide release was boosted by protonation of both imidazolyl moiety in IMZ and carboxylate in $HBTC^{2-}$, a process that stimulated the dissolution of the material. At an elevated pH, the abundant OH^- ions promoted the dissociation of a CP [59] due to nucleophilic attack on metal centers driving a release of IMZ ligand. Additionally, the formatted hydrogen bonds between the protonated carboxylate groups within $HBTC^{2-}$ might dissociate following the deprotonation process in alkaline conditions, further accelerating fungicide release. This dual pH-dependent properties highlights the potential of **PDCP1** for responsive fungicide delivery, offering enhanced release in challenging environments and demonstrating utility in long-term preventive applications [60]. The cumulative released rates values were further fitted to the zero-order equation, first-order equation, Higuchi equation (Figs. S3b and d in Supporting information), and Korsmeyer-Peppas equation (Fig. 3b) to model the fungicide release. Among these models, the Korsmeyer-Peppas equation exhibited the best fit (Table S6 in Supporting information), yielding a diffusion exponent ($n < 0.3$), which suggested that the release process of IMZ from **PDCP1** conformed to Fickian diffusion [61].

The bioactivity of the released IMZ and the suspension of **PDCP1** against the pathogenic fungus *C. gloeosporioides* was firstly evaluated using IMZ, $ZnSO_4$, and H_3BTC as controls. Fig. 4a illustrated the inhibitory effect of the IMZ solution, **PDCP1** supernatant and **PDCP1** suspension against the tested strain. The inhibition rates on the tested strain for all the three experiments exceeded 95 % at a concentration of 8 μg/mL (Fig. 4b), while $ZnSO_4$ and H_3BTC displayed weak antifungal activities with the inhibition rates at only 35 %–43 % (Fig. S5 in Supporting information). Calculations based on the Logistic model (Fig. S6 in Supporting information) demonstrated that IMZ exhibited notable inhibitory activity against the tested strain with a median EC_{50} value of 1.60 μg/mL. While, **PDCP1** supernatant showed an $EC_{50} = 0.72$ μg/mL (based on the active ingredient IMZ), and **PDCP1** suspension demonstrated an $EC_{50} = 0.71$ μg/mL (based on the active ingredient IMZ in the supernatant, Table S7 in Supporting information). The enhanced antifungal ability of **PDCP1** was due to the synergistic inhibition of $ZnSO_4$ and H_3BTC. Since the supernatant of a **PDCP1** suspension exhibited a similar antifungal activity in comparison with the suspended mixture, in following sections, the supernatants of the suspensions were evaluated to qualify the antifungal activities. In order to evaluate the impact of the tap water on the anti-fungal process of **PDCP1**, a comparative analysis was conducted by using mediums with tap water instead of ultrapure water. Fig. S7a (Supporting information) showed that the EC_{50} value was 0.71 μg/mL for **PDCP1** supernatant against *C. gloeosporioides.* The result was not significantly different from the EC_{50} observed in sterile water, suggesting that the tap water did not significantly affect the fungal inhibition effect of **PDCP1** supernatant.

Furthermore, the antifungal activities of IMZ solution and supernatant of **PDCP1** suspension were evaluated against *M. oryzae* and *A. nees* (Fig. S8a in Supporting information). Figs. S8b and d (Supporting information) showed that the inhibition rates (at a concentration of 8 μg/mL) of the IMZ solution and the supernatant were observed to be 95.12 % or 98.36 % for *M. oryzae* and almost 100.00 % for *A. nees*, respectively. Figs. S8c and e (Supporting information) demonstrated that the inhibitory rates of the supernatant exhibited enhanced efficacies at $EC_{50} = 0.92$ μg/mL on *M. oryzae* and $EC_{50} = 0.56$ μg/mL on *A. nees* in comparison with those of IMZ solution at $EC_{50} = 1.12$ μg/mL on *M. oryzae* and $EC_{50} = 1.16$ μg/mL on *A. nees*, indicating the broad-spectrum antifungal effect of **PDCP1**.

The antifungal activities of **PDCP1** were further evaluated in a management of strawberry anthracnose, which was caused by *C. gloeosporioides*, in pot experiments using strawberry leaves. Inhibitory effects on *C. gloeosporioides* were tested with the IMZ solution (200 μg/mL) and **PDCP1** suspension (with an IMZ active ingredient at 200 μg/mL). The experiments were conducted with the treatment group and the prevention group. For the treatment group, the pathogen was inoculated onto the strawberry leaves, followed by spraying the fungicides with time intervals of 24.0 h. After 3 days, the leaves of the control group showed visible darkening and distinct areas of pathogenicity (Fig. 4c, left), while, the treated leaves exhibited significantly reduced lesion areas. After 7 days, the lesion areas for the control, the IMZ solution, and **PDCP1** suspension groups further expanded to 4.92, 1.76, and 0.35 cm^2 (Fig. S9a in Supporting information), with inhibition rate at 68.85 % for the IMZ solution and at 92.85 % for **PDCP1** suspension (Fig. S9c in Supporting information). The prevention method is an alternative way to evaluate the efficacy of **PDCP1** in mitigating the infestation of the strain. Initially, the fungicides were introduced

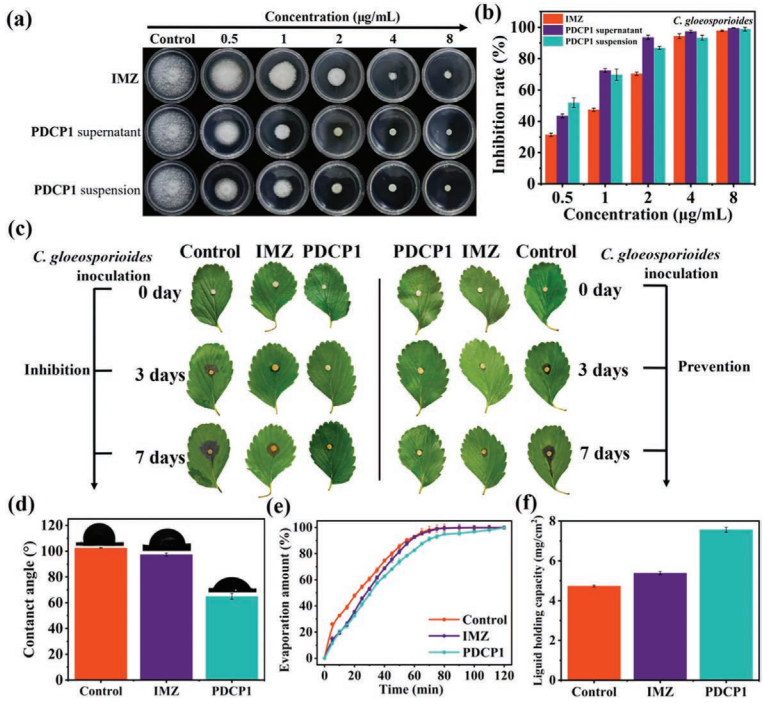


Fig. 4. (a) Photographs showing the inhibition effects of IMZ solution, **PDCP1** supernatant, **PDCP1** suspension, and the control against *C. gloeosporioides* and the corresponding inhibition rates (b) at concentrations of 0.5, 1, 2, 4, and 8 μg/mL. (c) Infection of *C. gloeosporioides* on strawberry leaves with either IMZ solution or **PDCP1** suspension, and digital photographs of strawberry leaves after treatment for inhibition and prevention. (d) Contact angle images of water, IMZ solution, and **PDCP1** suspension on strawberry leaves. (e) Evaporation of the water, IMZ solution, and **PDCP1** suspension with filter paper over time. (f) LHC of water, IMZ solution, and **PDCP1** suspension on strawberry leaves.

onto the leaves, 6.0 h later, *C. gloeosporioides* was inoculated on the tested leaves. After 7 days, the infected areas (Fig. 4c, right and Fig. S9b in Supporting information) and the inhibition rates (Fig. S9d in Supporting information) were 0.48 cm^2 and 85.88 % for the IMZ solution; 0.28 cm^2 and 91.76 % for **PDCP1** suspension. The results indicated that **PDCP1** suspension exhibited robust prevention and treatment ability towards strawberry anthracnose.

Leaf affinity or wettability was crucial for fungicide utilization [62], which can be evaluated by contact angle (CA) of a solution on the leaf surface. Fig. 4d showed the CAs of the control, the IMZ solution and **PDCP1** suspension on strawberry leaves in values of 102.58°, 97.39°, and 64.99°. The decrease in the angles for the suspension in comparison with the solution and the control might attribute to carboxylic acid groups in **PDCP1** suspension establish hydrogen bonds with the surface of strawberry leaves and enhanced adhesion of the material and contact area on the strawberry blade surface [63].

The effectiveness of fungicides was closely related to their residence time on leaf surfaces [64], and a slow volatilization rate of the solution on the leaves may prolong contact time of a pesticide with the target. In this experiment, the volatilization rates of the control, IMZ solution, and **PDCP1** aqueous suspension were evaluated using a filter paper method. As can be seen from Fig. 4e, the evaporation rates of the control group, the IMZ solution and **PDCP1** suspension were 60.60 %, 52.91 % and 48.65 %, respectively, at the 0.5 h mark. The slower volatilization rates for both IMZ solution and **PDCP1** aqueous suspension than that of the control group may attribute to reduce of the solvent vapor pressure of the solution and to elevate the boiling point resulting from the incorporation of the released solutes [65]. The aqueous suspension of **PDCP1** may have a more lasting effect, which could enhance the antifungal effect. In addition, the results demonstrate that the liquid holding capacity (LHC) of the pesticide solution is optimized following the addition of solutes in comparison to pure water (Fig. 4f). The LHC of the IMZ solution was 5.38 mg/cm^2, and following the introduction of **PDCP1**, the LHC increased by 40.73 % (7.56 mg/cm^2). This increase in LHC may be attributed to the interaction of **PDCP1** with the waxy components (alcohols, acids, aldehydes and other higher aliphatic compounds) on the plant leaves, which enhances the adhesion of the droplets to the leaves [65].

The process of photodegradation represented a significant factor contributing to the loss of fungicides during real application in agricultural fields [66]. A simulation experiment was therefore designed to evaluate the ultraviolet (UV) degradation of commercial IMZ (emulsion), IMZ solution and **PDCP1** suspension. As illustrated in Fig. 5a, after a 6.0 h exposure to the UV radiation, 96.40 % of the commercial IMZ and 99.12 % of the IMZ had undergone degradation. While, **PDCP1** was degraded only 50.34 %, much less than that of the free IMZ. The results indicated the immobilization of IMZ in the CP provided UV protection on IMZ, thereby potentially delaying the photolysis and prolonging the persistence of the fungicide under field conditions.

Considering the differences in decomposition process of IMZ solution and **PDCP1** suspension, UV–vis spectra of H_3BTC and IMZ solutions was first evaluated. UV–vis absorption of H_3BTC and IMZ solutions overlapped (Fig. S10 in Supporting information) at wavelength around 254 nm [67]. The competition in adsorption of incoming light may overshadow the irradiation and reduce the damage to IMZ molecules further reducing the decomposition. Furthermore, within the solid crystalline materials, a higher density of the IMZ may receive relative less incoming light to avoid UV induced decomposition of the IMZ molecules in comparison with the ones in the solution [68–70]. And, the solid state IMZ molecules in the crystalline material was enveloped, this might avoid to contact with oxygen and water, further, to avoid to be involve in oxygen, water and light induced decomposition process [71].

The storage stability was a major indicator to evaluate the quality of fungicide formulation [72,73]. Therefore, the thermal stor-

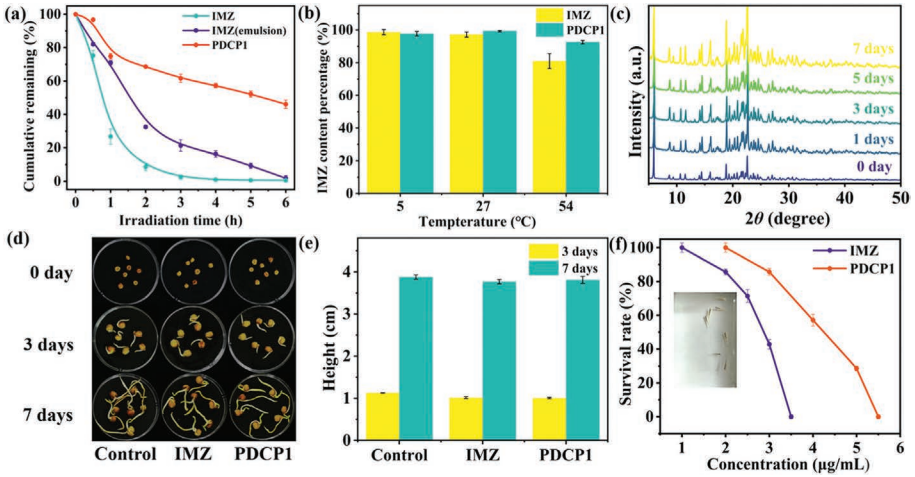


Fig. 5. (a) UV-resistance of IMZ emulsion, IMZ solution and **PDCP1** suspension. (b) Storage of solid IMZ and **PDCP1**. (c) Storage of **PDCP1** suspension. (d) Soybean seed germination, (e) seedling height, (f) zebrafish safety experiments with IMZ and **PDCP1**.

age of solid IMZ and **PDCP1** was evaluated at different temperatures (5, 27 and 54 °C), the content of the IMZ residual in the samples was examined by HPLC (Fig. 5b). The results demonstrated that after 7 days of storage, at 5 and 27 °C, both IMZ and **PDCP1** showed no significant decomposition, with IMZ residuals ranging from 97.54 % to 99.38 %. However, at the elevated temperature of 54 °C, the samples' decomposition was stimulated, as a result, the IMZ and **PDCP1** exhibited a 18.97 % and 6.24 % decline, respectively. So, **PDCP1** enhanced the thermal stability of immobilized IMZ in the structure.

In addition, the water stability of **PDCP1** was analyzed by evaluation of PXRD analysis of the sample (Fig. 5c) at times of 0, 1, 3, 5, and 7 days. All the P-XRD analysis results were consistent with each other, indicating no phase transition throughout the aqueous stability experiments. Overall, **PDCP1** demonstrated excellent UV resistance, along with both thermal and water stability.

Further research was investigated on the environmental hazards of fungicide application on non-target organisms. To evaluate the effects of IMZ (100 μg/mL) and **PDCP1** (with an IMZ active ingredient at 100 μg/mL) on seed germination, soybean seeds were selected as test organisms (Figs. 5d and e). Within a period of seven-day germination, the soybeans sprouts were divided into three groups. Those were treated with water, IMZ solution or **PDCP1** suspension, respectively. The results demonstrated average growth heights at 3.92 ± 0.16 cm as the control, 3.63 ± 0.15 cm for the solution and 3.78 ± 0.13 cm for the suspension. Both IMZ solution and **PDCP1** suspension showed a slight inhibitory effect on seedling germination due to the effect of IMZ. In addition, the seed germination test on the wheat seeds also demonstrated a similar result (Fig. S11 in Supporting information), indicating that both **PDCP1** and IMZ treatments inhibited wheat seedling height compared to the control, and the seedling heights from **PDCP1** group were significantly longer than that of the IMZ group.

Zebrafishes as a model organism were employed for environmental toxicological evaluation of the impact of the IMZ solution and **PDCP1** suspension. After a treatment of 96.0 h, zebrafishes (7 in each group) in the treatment groups displayed clear symptoms of acute toxicity (Fig. 5f), such as erratic swimming patterns, frequent tumbling, and loss of balance. The mortality rate rose as an increase of treated concentration, demonstrating a concentration-dependent relationship. After 96 h, the calculated LC_{50} of IMZ was 2.79 μg/mL, while that of **PDCP1** was 4.31 μg/mL.

The RAW264.7 mouse monocyte macrophage cell line was used as a mammalian cell model to assess the cytotoxicity of IMZ and **PDCP1**. Fig. S12 (Supporting information) showed that as the concentration of IMZ or **PDCP1** increased, the cell survival rates exhibited a dose-dependent decline, the 48.0 h LC_{50} values for IMZ and **PDCP1** were determined to be 1.87 and 5.47 μg/mL, respectively. In addition, RAW264.7 mouse cells data indicated that **PDCP1** exhibited low cytotoxicity against RAW264.7 cells within a specific concentration range, which did not induce cell death, and demonstrated favorable biosafety.

Biological safety experiments suggested that the immobilized IMZ in **PDCP1** reduced the real concentration of IMZ in the suspension so that reducing its toxicity in comparison with the IMZ solution. Furthermore, it was notable that the survival rate of RAW264.7 cells was marginally higher than that of the control group at a low concentration (0.3125 μg/mL). This may be attributed to the release of Zn(II) fragments from **PDCP1**, which may have a stimulatory effect on cell proliferation [74].

IMZ as a major component of **PDCP1**, which primarily inhibits the activity of sterol 14α-demethylase P450 (CYP51) and disrupts the cell membrane of fungi, thereby inhibiting fungal growth [47]. To gain further insight into the micro-morphological changes occurring in *C. gloeosporioides* in response to **PDCP1**, the alterations to the mycelium prior to and following the application of the treatment were observed using SEM. It can be observed that the mycelium of the fungus in the control group exhibited a firm structure and uniform diameter, displaying a plump, smooth, and complete morphology (Fig. S13a in Supporting information). In contrast to the control group, the mycelium treated with 2 μg/mL **PDCP1** exhibited deformation, a rough surface, and severe breakage (Fig. S13b in Supporting information). These results supported/indicated that **PDCP1** impeded the growth of *C. gloeosporioides* by damaging the mycelial structure. Further considering the mechanisms of the antifungal effect of **PDCP1** on *C. gloeosporioides*, surface charges of the fungus fluids was concerned. The zeta potentials of the fungus and **PDCP1** were -3.62 ± 0.13 mV and 6.54 ± 0.23 mV, respectively, the opposite in zeta potential values may cause electrostatic adsorption between fungal hyphae and the particles so that contribution to a fungicidal effect. It was hypothesized that the antifungal activity of **PDCP1** may depend on electrostatic adsorption for sterilization [75].

In summary, a successful preparation of coordination polymer $[Zn(HBTC)(IMZ)_2]_n$ (**PDCP1**) by combining of Zn(II), IMZ and H_3BTC *via* static and stirred solvothermal method was presented. Especially, by a simply stir at room temperature, high rate of IMZ (68.1 %) in the CP was loaded to achieve the nano-sized material (179 nm). The solid-state structure information was described, the intermolecular interactions and their contribution to crystal

packing were studied by supermolecules, Hirshfeld, Fingerprint plot and Mayer bond order. The prepared **PDCP1** exhibited pH-responsive controlled release properties in aqueous delivery system. In comparison with pure IMZ, **PDCP1** suspension demonstrated more stable UV-stability, storage stability, superior leaf wettability, and longer lasting volatility. Regarding of the inhibition of fungal growth, **PDCP1** supernatant was observed to significantly elevate the inhibitory effects of IMZ against strains of *C. gloeosporioides* ($EC_{50} = 0.72\,\mu g/mL$), *M. oryzae* ($EC_{50} = 0.92\,\mu g/mL$) and *A. nees* ($EC_{50} = 0.56\,\mu g/mL$). Biosafety evaluation results showed that **PDCP1** exhibited better bio-safety in seed germination, zebrafishes, and mouse cells (RAW264.7) than a single ingredient of IMZ. This work offers a straightforward method for syntheses of nano-fungicide coordination polymer, and demonstrates significant potential for addressing the issue of efficient fungicide utilization.

Declaration of competing interest

The authors declare that they have no known competing financial interests or personal relationships that could have appeared to influence the work reported in this paper.

CRediT authorship contribution statement

Gao-Sheng Zhu: Writing – original draft, Visualization, Validation, Software, Methodology, Investigation, Formal analysis, Data curation, Conceptualization. **Zhen-Hang Xu:** Software, Formal analysis, Data curation. **Shao-Zhan Lan:** Software, Formal analysis, Data curation. **Long Li:** Validation, Methodology, Formal analysis. **Yan-Ying Zheng:** Validation, Methodology, Data curation. **Lu Zhang:** Visualization, Software, Data curation. **Qiao-Xia Shang:** Visualization, Validation, Data curation. **Bao-Yi Yu:** Writing – review & editing, Validation, Supervision, Resources, Funding acquisition, Conceptualization. **Chong-Chen Wang:** Writing – review & editing, Supervision, Conceptualization.

Acknowledgment

This work was supported by Beijing Innovation Consortium of Agriculture Research System (No. BAIC01).

Supplementary materials

Supplementary material associated with this article can be found, in the online version, at doi:10.1016/j.cclet.2025.111428.

References

[1] K. Zhou, Z. Shi, X.H. Yi, et al., Chin. Chem. Lett. 36 (2024) 110226.
[2] C.Y. Wang, Y.Q. Liu, C. Jia, et al., Chin. Chem. Lett. 34 (2023) 108400.
[3] W. Fu, X. Hu, Q. Yuan, et al., Chin. Chem. Lett. 34 (2023) 108064.
[4] J. Liu, X. Zhu, X. Chen, et al., Environ. Sci. Nano 7 (2020) 210–227.
[5] S. Liu, L. Pang, X. Wu, et al., Microchem. J. 202 (2024) 110782.
[6] M. Tavassoli, A. Khezerlou, M.A. Sani, et al., Int. J. Biol. Macromol. 259 (2024) 129182.
[7] C. Sun, Y. Zhang, Y. Dai, et al., J. Mol. Liq. 371 (2023) 121108.
[8] T.M. Abdalla, M.A. Adam, S.A. Onaizi, Surf. Interfaces 55 (2024) 105272.
[9] Z. Li, K. Tong, H. Dong, et al., Angew. Chem. Int. Ed. 64 (2025) e202502390.
[10] L. Lv, F. Jia, M. Deng, et al., Sci. Total Environ. 926 (2024) 172022.
[11] R. Hazime, Q.H. Nguyen, C. Ferronato, et al., Appl. Catal. 132-133 (2013) 519–526.
[12] N. Qisse, M. El Alouani, L. El Azzouzi, et al., Groundw. Sustain. Dev. 11 (2020) 100468.
[13] S.J. Phukan, S. Goswami, N.K. Sah, et al., Mater. Today Energy 46 (2024) 101703.
[14] M.D.H. Prodhan, M.A.R. Choudhury, N.K. Dutta, et al., J. Food Compost. Anal. 125 (2024) 105742.
[15] C.V. Papazlatani, M. Kolovou, E.E. Gkounou, et al., Environ. Pollut. 301 (2022) 119030.
[16] A.M. Silva, C. Martins-Gomes, S.S. Ferreira, et al., Int. J. Mol. Sci. 23 (2022) 8107.
[17] S.V. Prudnikova, N.G. Menzianova, S.A. Pyatina, et al., Physiol. Mol. Plant Pathol. 128 (2023) 102166.
[18] S. Jeanmart, J. Gagnepain, P. Maity, et al., Bioorg. Med. Chem. 26 (2018) 2009–2016.
[19] H. Karimi-Maleh, M. Ghalkhani, Z. Saberi Dehkordi, et al., J. Ind. Eng. Chem. 129 (2024) 105–123.
[20] R.S. Riseh, M. Vatankhah, M. Hassanisaadi, J.F. Kennedy, Int. J. Biol. Macromol. 269 (2024) 132079.
[21] D. Xiao, H. Wu, Y. Zhang, et al., J. Control. Release 352 (2022) 288–312.
[22] A.P. Keinath, Crop Prot. 106 (2018) 72–78.
[23] C. Huang, M. Cui, T. Li, et al., J. Hazard. Mater. 484 (2025) 136725.
[24] S.S. Li, S.M. Fang, J. Chen, et al., Sci. Total Environ. 864 (2023) 161050.
[25] S. Lu, B. Liang, J. Hu, et al., Chem. Eng. J. 482 (2024) 148990.
[26] P. Du, G. Chen, P. Zhang, et al., Ecotoxicol. Environ. Saf. 265 (2023) 115515.
[27] P. Santhoshkumar, D. Vikraman, K. Karuppasamy, et al., Appl. Surf. Sci. 661 (2024) 160075.
[28] J. Zhou, G. Liu, Z. Guo, et al., Chem. Eng. J. 455 (2023) 140167.
[29] Z. Jiang, K. Tong, Z. Li, et al., Angew. Chem. Int. Ed. 64 (2025) e202500791.
[30] P. Zhao, L. Cao, C. Wang, et al., Chemosphere 307 (2022) 135702.
[31] W. Zhang, R. Taheri-Ledari, M. Saeidirad, et al., J. Environ. Chem. Eng. 10 (2022) 108836.
[32] H. Chu, Z. Huang, G. Shen, et al., Environ. Sci.: Nano 12 (2025) 2901–2910.
[33] Z. Chavoshpour-Natanzi, N. Farzi, Surf. Interfaces 59 (2025) 105933.
[34] Z. Qin, J. Wei, Y. Wu, et al., Results Eng. 24 (2024) 103184.
[35] H. Li, Y. Liu, X. Zhu, et al., Energy Storage Mater. 73 (2024) 103859.
[36] C. Hou, N. Wei, Q. Liang, et al., Pest. Manag. Sci. 81 (2024) 798–808.
[37] L. Yang, H. Chen, Q. Zheng, et al., Chem. Eng. J. 458 (2023) 141417.
[38] D. Kobayashi, A. Hamakawa, Y. Yamaguchi, et al., Dalton Trans. 50 (2021) 7176–7180.
[39] S. Sujatha, N. Rajamohan, S. Sanjay, et al., Environ. Res. 246 (2024) 118018.
[40] J. Zuo, H. Yan, R. Lan, et al., Ind. Crops. Prod. 213 (2024) 118464.
[41] D. Han, F. Meng, J. Li, et al., Eur. Polym. J. 215 (2024) 113196.
[42] Y. Yin, M. Yang, J. Xi, et al., Carbohydr. Polym. 247 (2020) 116677.
[43] A. Kathuria, A. El Badawy, S. Al-Ghamdi, et al., Trends Food Sci. Tech. 138 (2023) 323–338.
[44] P. Gao, S. Mukherjee, M.Z. Hussain, et al., Chem. Eng. J. 492 (2024) 152377.
[45] C. Cano-Sarmiento, D.I. Téllez-Medina, R. Viveros-Contreras, et al., Food Eng. Rev. 10 (2018) 113–138.
[46] P. Du, J. Wang, G. Sun, et al., Water Res. 212 (2022) 118113.
[47] C. Savage, A. Erasmus, W. du Plooy, et al., Postharvest Biol. Technol. 219 (2025) 113227.
[48] H. Li, Q. Lu, J. Shi, et al., Adv. Funct. Mater. 34 (2023) 2309383.
[49] S.K. Seth, CrystEngComm 15 (2013) 1772.
[50] A. Chinthamreddy, R. Karreddula, G.K. Pitchika, et al., J. Inorg. Organomet. Polym. Mater. 31 (2020) 1381–1394.
[51] P.R. Spackman, M.J. Turner, J.J. McKinnon, et al., J. Appl. Crystallogr. 54 (2021) 1006–1011.
[52] Z.U.H. Bhat, A. Abbasi, S. Hanif, et al., Inorg. Chem. Commun. 143 (2022) 109810.
[53] X. Wang, Y. Wu, Y. Rui, et al., J. Mol. Struct. 1312 (2024) 138493.
[54] N. Dissem, N. Ferhi, T. Maris, et al., J. Mol. Struct. 1254 (2022) 132317.
[55] L.B.d.O. Freitas, L.d.M. Corgosinho, J.A.Q.A. Faria, et al., Microporous Mesoporous Mater. 242 (2017) 271–283.
[56] F. He, Q. Zhou, L. Wang, et al., Appl. Clay Sci. 183 (2019) 105347.
[57] C. Valverde, G. Lligadas, J.C. Ronda, et al., Polym. Degrad. Stab. 155 (2018) 84–94.
[58] W. Cai, J. Wang, C. Chu, et al., Adv. Sci. 6 (2019) 1801526.
[59] K. Wang, Y. Li, L.H. Xie, et al., Chem. Soc. Rev. 51 (2022) 6417–6441.
[60] M.N. Jahan, M.A. Alam, M.M. Rahman, et al., RSC Adv. 14 (2024) 23560–23573.
[61] X. Zhang, X. Tang, C. Zhao, et al., Chem. Eng. J. 431 (2022) 133351.
[62] S. Song, M. Wan, W. Feng, et al., Langmuir 38 (2022) 10867–10874.
[63] N. Ma, H. Lin, L. Ning, et al., J. Clean. Prod. 429 (2023) 139536.
[64] Y. Liu, D. Kong, G. Tang, et al., Colloids Surf. B 242 (2024) 114077.
[65] Y.T. Xiao, C.H. Wu, S.S. Feng, et al., Chem. Eng. J. 475 (2023) 146037.
[66] X.X. Xu, X.D. Shi, B.B. Wang, et al., Chem. Eng. J. 485 (2024) 150061.
[67] L. Hao, L. Gong, L. Chen, et al., Chem. Eng. J. 396 (2020) 125233.
[68] T. Lu, E. Solis-Ramos, Y. Yi, et al., Polym. Degrad. Stab. 154 (2018) 203–210.
[69] N. Zhang, Y. Xiao, S. Hu, et al., Chem. Eng. J. 500 (2024) 157351.
[70] P. Du, W. Liu, Q. Zhang, et al., Water Res. 232 (2023) 119676.
[71] H.D. Burrows, M. Canle L, J.A. Santaballa, et al., J. Photoch. Photobio. B 67 (2002) 71–108.
[72] S. Zhi, A. Liang, Z. Jiang, J. Environ. Chem. Eng. 11 (2023) 111276.
[73] F. Peng, X. Wang, W. Zhang, et al., Nanomaterials 12 (2022) 1112.
[74] H.J. Zhao, X.H. Zhao, Biol. Trace Elem. Res. 192 (2019) 287–296.
[75] J. Zhou, M. Zhai, R. Wang, et al., Compos. A: Appl. Sci. Manuf. 161 (2022) 107080.